BULLETIN DE L'ASSOCIATION MINERALOGIQUE DU CANADA

THE CANADIAN MINERALOGIST

JOURNAL OF THE MINERALOGICAL ASSOCIATION OF CANADA

Volume 31 March 1993 Part 1

Canadian Mineralogist
Vol. 31, pp. 1-17 (1993)

ARSENIAN PYRITE FROM GOLD DEPOSITS: Au AND As DISTRIBUTION INVESTIGATED BY SIMS AND EMP, AND COLOR STAINING AND SURFACE OXIDATION BY XPS AND LIMS

MICHAEL E. FLEET
Department of Geology, University of Western Ontario, London, Ontario N6A 5B7

STEPHEN L. CHRYSSOULIS
Surface Science Western, University of Western Ontario, London, Ontario N6A 5B7

PETER J. MacLEAN
Department of Geology, University of Western Ontario, London, Ontario N6A 5B7

ROSS DAVIDSON AND CHRISTOPHER G. WEISENER
Surface Science Western, University of Western Ontario, London, Ontario N6A 5B7

ABSTRACT

Ion-probe microanalysis and ion mapping by SIMS have established that submicroscopic ppm-levels of gold in arsenian pyrite from stratabound and stratiform gold deposits are associated exclusively with As-rich growth bands; the gold is most probably incorporated in solid solution in arsenian pyrite *via* As-rich growth surfaces. The nature of the composition-specific stain resulting from oxidation of polished surfaces of pyrite-group minerals with potassium permanganate solution (in 1:1 sulfuric acid) has been studied by X-ray photoelectron spectroscopy (XPS) and laser ionization mass spectrometry (LIMS). The surface layers of stained sections of arsenian pyrite and arsenopyrite contain three species of sulfur (disulfide, elemental S, and sulfate), and the proportion of elemental S in surface layers of pyrite increases with As content of the substrate. The amount of Mn present in surface layers is insignificant. Therefore, stain color is attributed to optical interference by a thin surface-layer of elemental S. Surface oxidation of pyrite by potassium permanganate solution is promoted by As-for-S substitution; in this way, color development can be correlated with the distribution of As and "invisible" Au.

Keywords: pyrite, "invisible" gold, arsenian pyrite, Au by ion-probe microanalysis, ion mapping by SIMS, surface oxidation of pyrite, X-ray photoelectron spectroscopy of pyrite, surface films.

SOMMAIRE

L'analyse à la microsonde ionique et la "cartographie ionique" par spectrométrie de masse des ions secondaires ont établi la présence de quantités d'or submicroscopiques à des niveaux du ppm, associées exclusivement aux zones de croissance riches en

As dans la pyrite arsenifère provenant de gisements d'or syn-sédimentaires et stratiformes. L'or serait tout probablement incorporé en solution solide dans la pyrite arsenifère par le biais de surfaces de croissance enrichies en As. Nous avons étudié la nature de la coloration révélatrice de la composition dans les minéraux du groupe de la pyrite, résultat de l'oxydation de surfaces polies exposées à une solution de permanganate de potassium (dans l'acide sulfurique 1:1), au moyen de la spectroscopie des photo-électrons délogés par les rayons X et par ionisation au laser avec spectrométrie de masse. Les couches de surface ternies développées sur la pyrite arsenifère et sur l'arsenopyrite contiennent trois espèces de soufre, soient bisulfure, soufre élémentaire, et sulfate; la proportion du soufre élémentaire dans les couches de surface de la pyrite augmente avec la teneur en As du substrat. La quantité de Mn dans les couches de surface est infime. C'est donc dire que la couleur de cette ternissure dépend d'une interférence optique causée par une mince couche de soufre en surface. L'oxydation de la pyrite en surface par la solution de permanganate de potassium augmente avec le degré de remplacement du soufre par l'arsenic. De cette façon, le développement de la couleur montre une corrélation avec la distribution de l'arsenic et de l'or dit "invisible".

(Traduit par la Rédaction)

Mots-clés: pyrite, or "invisible", pyrite arsenifère, analyse par microsonde ionique, cartographie des ions, spectrométrie de masse des ions secondaires, oxydation de surface, spectroscopie des photo-électrons émis par les rayons X, films de surface.

Introduction

Gold deposits hosted by sedimentary and volcanic rocks characteristically have anomalous contents of As, present as arsenopyrite, As-bearing pyrite, native As, realgar, and orpiment. The content and spatial distribution of As in pyrite associated with gold mineralization were investigated systematically by Fleet *et al.* (1989) and MacLean (1991). It was noted that arsenian pyrite is associated with gold deposits that are stratabound and stratiform and whose host rocks have not been metamorphosed beyond middle low-grade conditions. Pyrite grains from such deposits are commonly oscillatory zoned in As content on a fine (micrometer) scale; maximum As contents, in As-rich bands, attain 4 to 8 wt.%, as determined by electron-microprobe analysis. Oscillatory-zoned arsenian pyrite has been reported also from other parageneses (Burkart-Baumann & Ottemann 1971, Arnold 1981, references in Fleet *et al.* 1989). The oscillatory-zoned microstructures of arsenian pyrite from gold deposits were interpreted by Fleet *et al.* (1989) as a growth feature and attributed to episodic fluctuation in fluid composition during crystal growth.

The spatial variation in the content of As in pyrite is resolved by surface staining of polished sections with a solution of potassium permanganate in dilute (1:1) sulfuric acid (Fleet *et al.* 1989). As confirmed by electron-microprobe analysis, the color of a stained area is proportional to its As content. This technique has proven useful to understand the complex history of fluids associated with stratabound and stratiform gold deposits; the stain commonly reveals an initial generation of framboidal or sector-zoned pyrite, a phase of very-fine-scale episodic variation in solution chemistry resulting in a zonal stratigraphy, as in sphalerite of Mississippi-Valley-type and epithermal deposits (*e.g.*, Barton *et al.* 1977, Barton & Bethke 1987), dissolution, brecciation, replacement, and late overgrowths of As-poor pyrite. Furthermore, MacLean & Fleet (1989) used the surface staining procedure to show that the compact rounded pyrite grains in quartz-pebble conglomerate gold ore from the Witwatersrand basin of South Africa are indeed detrital in origin, and thus provided further evidence for a detrital origin for this important class of gold deposit.

Using ion-probe microanalysis (secondary ion mass spectrometry, SIMS), Cook & Chryssoulis (1990) demonstrated a positive correlation between the concentration of As and "invisible" Au in arsenian pyrite. "Invisible" gold is defined as gold present either in solid solution or as particles below resolution by SEM in the back-scattered electron mode. More recently, Griffin *et al.* (1991) analyzed arsenian pyrite from the North Arm epithermal Ag–Au deposit, in Queensland, Australia, for *in situ* contents of Cu, Sb, Se, Ag, Zn, Pb and Mo by proton microprobe. They reported that the spatial distributions of Cu, Sb and Se broadly correlate with As content. However, the gold contents of the North Arm arsenian pyrite was found to be below the levels of detection by proton microprobe (20–25 ppm: Cabri *et al.* 1991).

In the present paper, we use SIMS and electron-microprobe (EMP) analysis to show that the spatial distribution of "invisible" Au in arsenian pyrite correlates with As content, as mapped by color staining and EMP back-scattered electron images. A more detailed study of the distribution of "invisible" gold in pyrite using ion-probe microanalysis and ion mapping by SIMS is presented elsewhere (Chryssoulis & Weisener 1991). In addition, in this paper, the nature of the stain resulting from surface oxidation of arsenian pyrite with potassium permanganate solution is investigated by X-ray photoelectron spectroscopy (XPS) and laser-ionization mass spectrometry (LIMS). The XPS study leads to interesting observations on the surface oxidation of pyrite.

Samples and Analytical Procedures

Samples

All samples were taken from the mineral deposits and

mineral collections at the University of Western Ontario, and included arsenian pyrite from the Agnico-Eagle mine, Joutel, Quebec (samples 19560, 19567) and the Fairview mine, South Africa (17359), As-poor pyrite from the Horne mine, Noranda, Quebec (2040) and an unknown locality (394), arsenopyrite from Deloro, Ontario (3388) and Zacatecas, Mexico (2486), and löllingite from the LaRose mine, Cobalt, Ontario.

The geology and pyrite mineralogy of the Agnico-Eagle and Fairview mines were reviewed in Fleet *et al.* (1989) and MacLean (1991). The Agnico-Eagle gold deposit is a stratabound-stratiform body associated with felsic pyroclastic, carbonate, and clastic sedimentary rocks of the Gale Group of the Archean, Abitibi greenstone belt. Gold is associated with a fine-grained banded pyrite within an Fe-rich carbonate unit and with coarse-grained poikiloblastic pyrite in a chloritic rock adjacent to a diabase dike (Barnett *et al.* 1982). The pyrite within the Fe-rich carbonate unit is arsenian, and is characterized by elaborate optical microstructures with fine-scale oscillatory zoning in As content. The Fairview gold mine is located 12 km east of Barberton in East Transvaal, South Africa, and also is Archean in age. Gold ore occurs as sulfidic reefs of disseminated to massive pyrite and arsenopyrite in concordant bodies and discordant fractures in graywackes and shales of the lower Fig Tree Group, and quartz reefs of discrete quartz-filled fractures in the brittle quartzite horizon of the Moodies Group (Wiggett *et al.* 1986). Pyrite from the sulfidic reefs is arsenian and characterized by optical microstructures even more elaborate than those of arsenian pyrite from the Agnico-Eagle mine.

Grains of arsenian pyrite were selected by hand separation from crushed samples under a binocular microscope. Samples for SIMS analysis were prepared as polished grains set in 25-mm-diameter blocks of epoxy with up to 40 wt.% graphite added. Samples for XPS analysis were prepared similarly in 18-mm-diameter blocks. The LIMS analyses were made with standard 25-mm-diameter polished thin sections.

All polished blocks and sections were stained with a solution of $KMnO_4$ in 1:1 H_2SO_4 before analysis by EMP, SIMS, XPS, and LIMS. The stain solution was prepared as required and applied drop-wise with a stirring rod on cleaned polished surfaces. Some experimentation was required to find the optimum conditions for staining, and treatment times typically varied from 30 seconds to 5 minutes. Stained sections were washed in tap water to stop reaction and dried in an air jet. Stain colors are most visible in air (*i.e.*, when the stained surface is not in contact with water), and range through orange, brown, red, purple, blue and white with increasing As content and treatment time (*e.g.*, see below, Fig. 3a).

Secondary Ion Mass Spectrometry (SIMS)

The samples were analyzed using a Cameca IMS–3f ion microscope for ^{197}Au, ^{75}As, ^{56}Fe and ^{34}S. All measurements were made with a cesium primary beam of about 500 nA at 14.1 keV while monitoring negative ions. For ion-probe microanalysis, the area analyzed is defined by a set of apertures in the secondary column. All present analyses were made with an aperture of 60 μm. Iron and S were determined to monitor instrumental conditions during the analysis and for standardization. SIMS has been used routinely to quantify the "invisible" Au content and colloidal-size Au in pyrite and arsenopyrite (Cook & Chryssoulis 1990). Gold was quantified using the external standardization procedure (Chryssoulis 1990). Molecular ions were eliminated by voltage offsetting: 180 V, fully open energy-slits for microprobe analysis (Chryssoulis 1990) and 80 V, one-tenth-open slits for imaging (Chryssoulis & Weisener 1991). With a 10-s counting time for Au, the limit of detection in pyrite is 0.4 ppm Au, with an accuracy of about 10–15% (Chryssoulis *et al.* 1987). The SIMS microprobe results are summarized in Figures 1a, b for pyrite grains from the Agnico-Eagle and Fairview mines, respectively.

Ion mapping was used to determine the distribution of Au and As within individual grains. Ion imaging was performed by electronically rastering the primary beam over an area of 250×250 μm^2. Images obtained on the dual channel plate were captured by a Cohu solid-state camera and processed by an image-processing system developed at Surface Science Western. The size of the cesium beam at 500 nA is 150 μm, but the effective spatial resolution in the resulting images is about 2 μm. Other details on the present procedure of ion mapping are given in Chryssoulis & Weisener (1991). Maps showing the distribution of ^{197}Au and ^{34}S ions are given in Figures 2b and 3c. In Figure 2b, the distribution of "invisible" Au follows closely the very-fine-scale variation in As distribution depicted in the back-scattered electron image (Fig. 2a). Zones with high content of "invisible" Au (color-coded orange) in a 0.5-mm subhedral grain of pyrite from the Fairview mine follow growth zones of an earlier generation of euhedral arsenian pyrite that has been overgrown by later Au- and As-poor pyrite (Fig. 3c).

Electron-Microprobe (EMP) Analysis

The samples of pyrite used for SIMS analysis were analyzed by EMP for Fe, S, As, Co, Ni, and Au using a JEOL JXA–8600 Superprobe, operated at 20 kV, 50 nA, with natural pyrite (Fe, S), arsenopyrite (As), synthetic NiS (Ni), and pure Co and Au as standards. The precision and reliability of the Au analyses were increased by using the Au$M\alpha$ line, 100-s counts, and one spectrometer dedicated entirely to Au, thus eliminating the possibility of crystal-positioning error. The detection limit for Au was estimated to be approximately 200 ppm, and systematic analysis of the As-poor pyrite standard gave

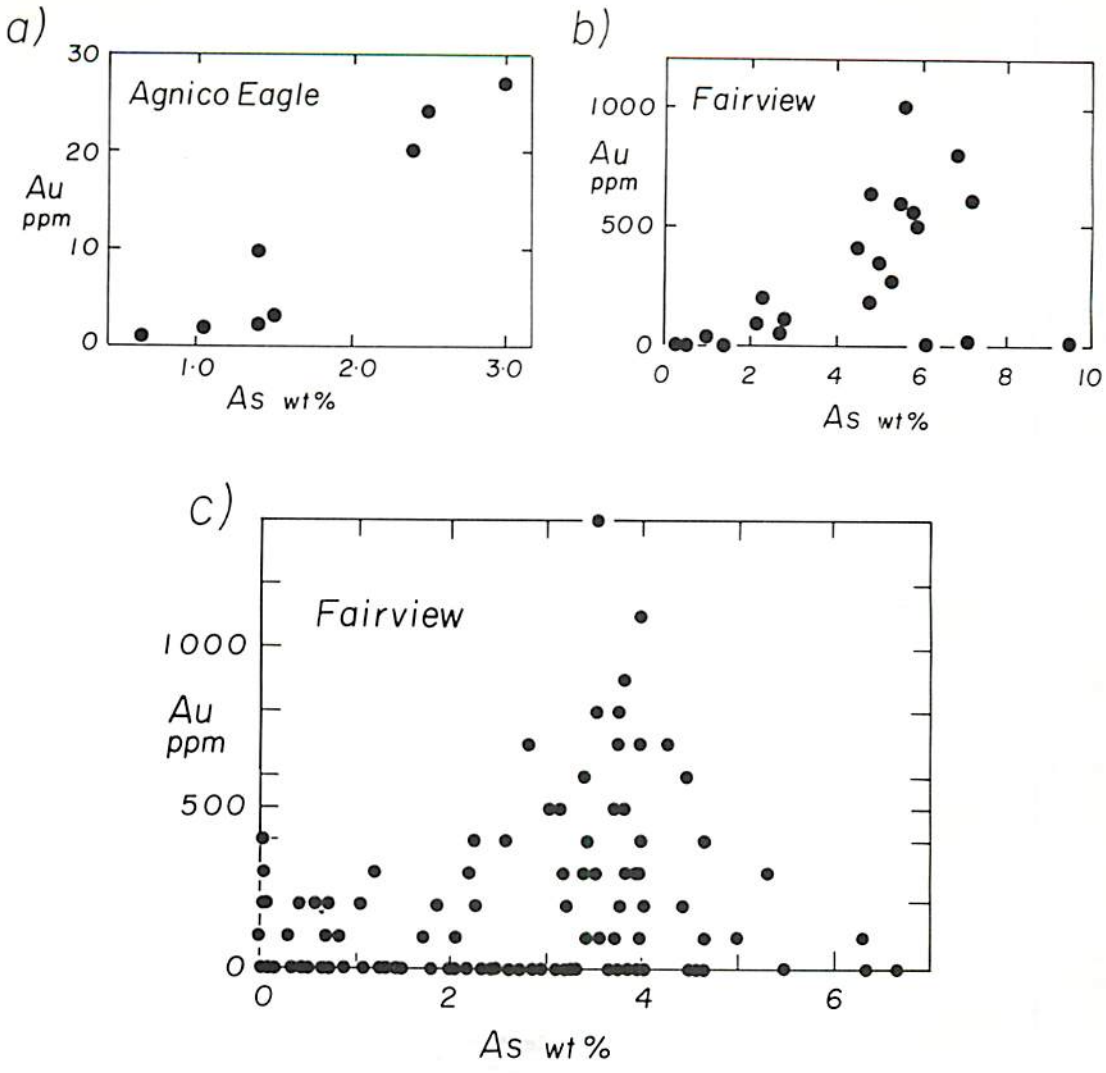

FIG. 1. Concentration of Au *versus* As in arsenian pyrite by ion-probe microanalysis; a) Agnico-Eagle mine (sample 19567), values for two grains, one of which is illustrated in Fig. 2; b) Fairview mine (sample 17359), values for four grains, one of which is illustrated in Fig. 3b, and c) by electron microprobe (EMP) analysis, Fairview mine (sample 17359), single grain illustrated in Fig. 3b.

values consistently less than 100 ppm, results comparable to those found by Cabri *et al.* (1989). Results are summarized in Figures 1c and 2a. Significant concentrations of gold (above 200 ppm) were essentially limited to the As-rich growth bands of the grain shown in Figures 3b and 3c.

The Co and Ni contents of the pyrite samples were as follows: sample 19560: Co 0.05 wt.%, Ni not detected (n.d.); sample 19567: Co 0.10, Ni 0.06; sample 17359: Co 0.07, Ni 0.0–0.4; sample 2040: Co 0.07, Ni n.d. and sample 394: Co 0.05, Ni n.d. With the exception of a single, very As-rich zone of the Fairview sample, the spatial variations of Co and Ni do not seem related to the variation in As content, and therefore these generally low contents were considered to be insignificant in the present context.

X-ray Photoelectron Spectroscopy (XPS)

X-ray photoelectron spectroscopy is a surface-sensitive technique that gives information on chemical state and surface composition. The theory of XPS was

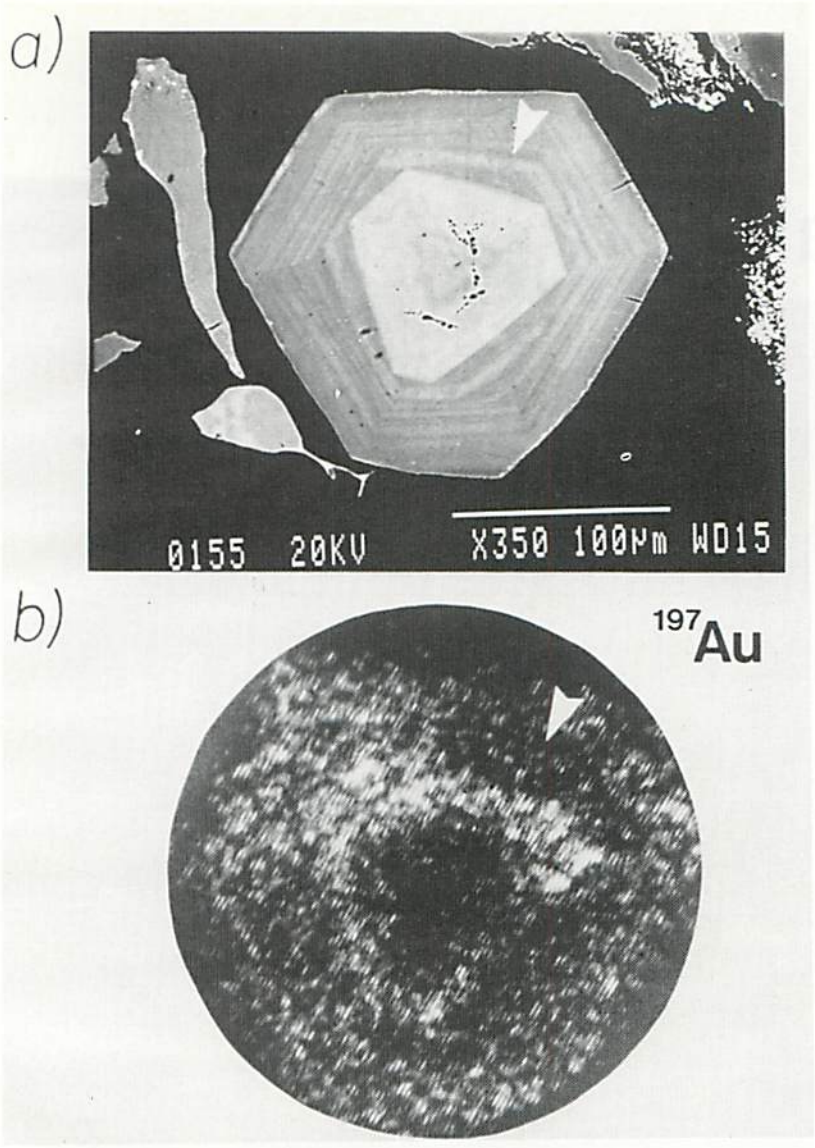

FIG. 2. a) EMP back-scattered electron image, and b) corresponding ^{197}Au ion map by SIMS for arsenian pyrite from the Agnico-Eagle mine (sample 19567); see Fig. 1a.

reviewed by Briggs & Seah (1983) and McIntyre (1984), and recent applications to pyrite include Jean & Bancroft (1985), Hyland & Bancroft (1989), and Mycroft *et al.* (1990). Briefly, and following Hyland & Bancroft (1989), monochromatic X rays with energy E_X are used to eject core electrons from surface atoms. By measuring the kinetic energy (K.E.) of the electrons ejected from the core, their binding energy (B.E.) in the surface layer can be determined from

$$\text{B.E.} = E_X - \text{K.E.} \quad (1)$$

Binding energy depends on chemical state: the 2–, 1– (disulfide), 0, and 6+ oxidation states of sulfur have approximate binding energies of 161, 162.4, 163.8, and 169.0 eV, respectively, varying slightly with chemical combination. The number of electrons ejected from the core is proportional to surface composition; hence, peak areas in the energy spectrum (*e.g.*, Fig. 4) reflect the proportion of oxidation (chemical) states occupied in the

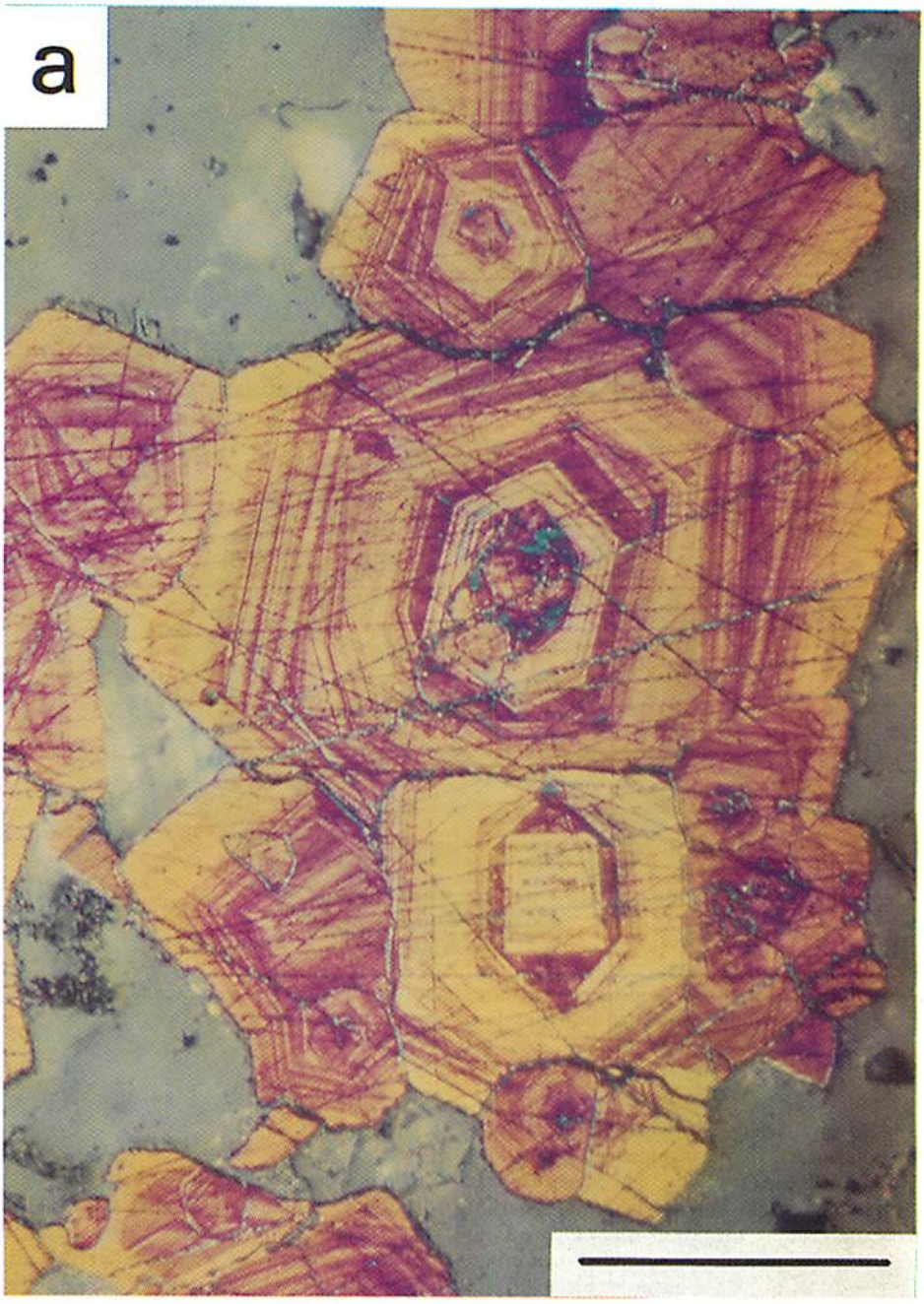

FIG. 3a. Optical micrograph of arsenian pyrite grains from Fe carbonate unit of Agnico-Eagle mine, stained with $KMnO_4$ and showing As-rich growth bands (purple). Scale bar is 0.1 mm.

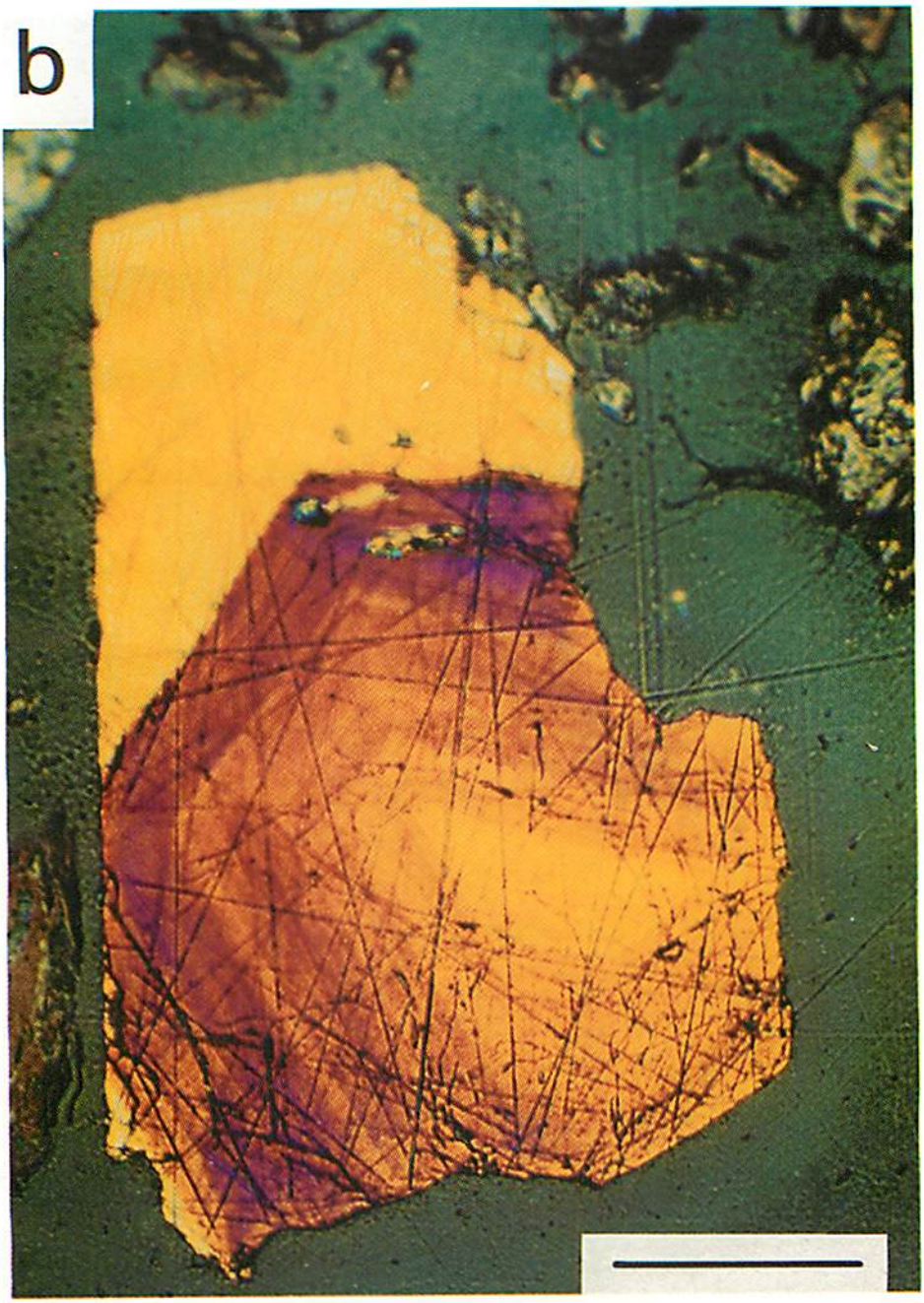

FIG. 3b. Arsenian pyrite grain from sulfidic reef of Fairview mine (sample 17359). Optical micrograph of polished section stained with $KMnO_4$ and showing As-rich growth bands (purple, red). Scale bar is 0.1 mm.

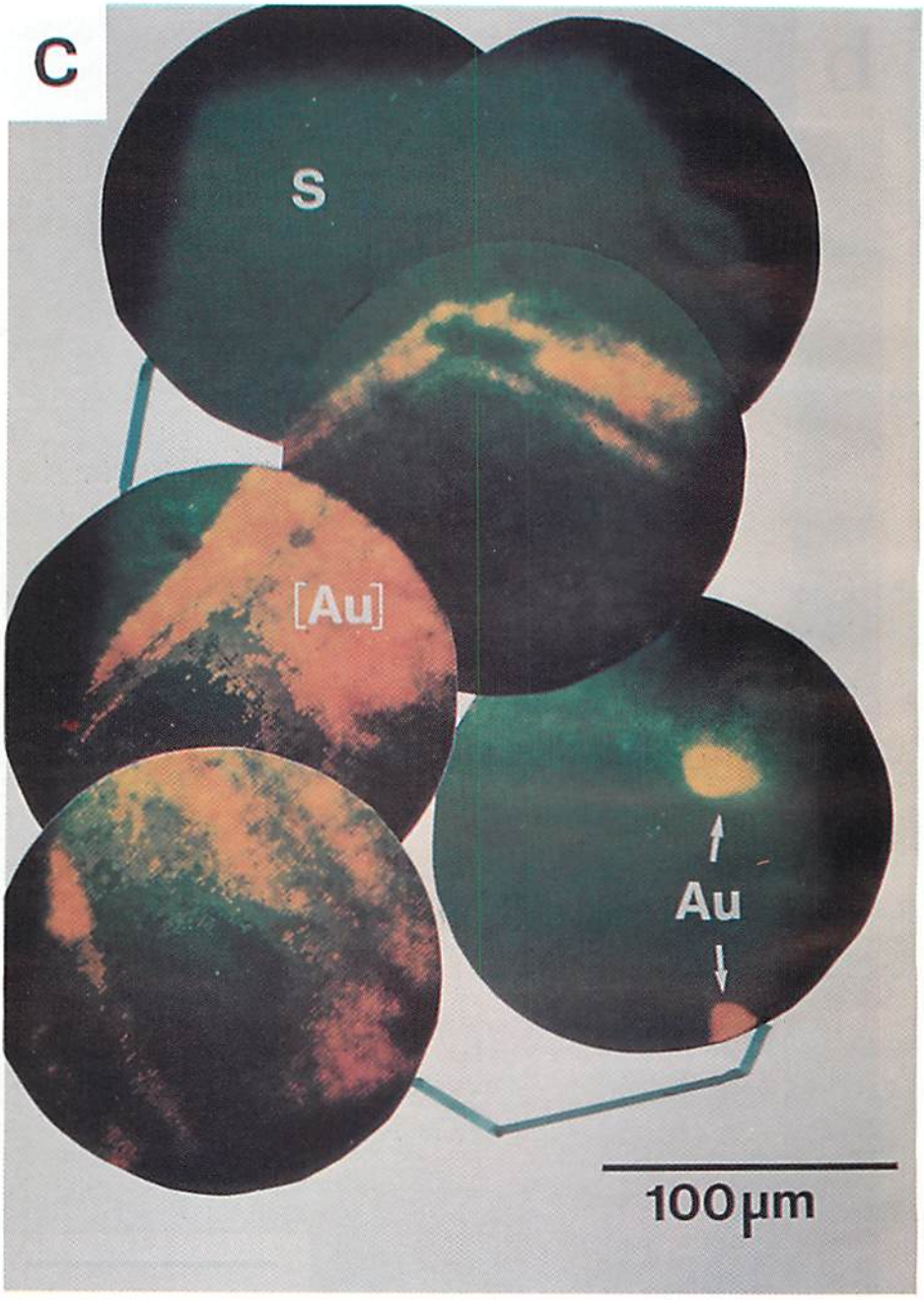

FIG. 3c. Arsenian pyrite grain from sulfidic reef of Fairview mine (sample 17359). Combined ^{34}S (green) and ^{197}Au (yellow) ion map obtained by SIMS; two small particles of metallic gold are labeled "Au". Scale bar is 0.1 mm.

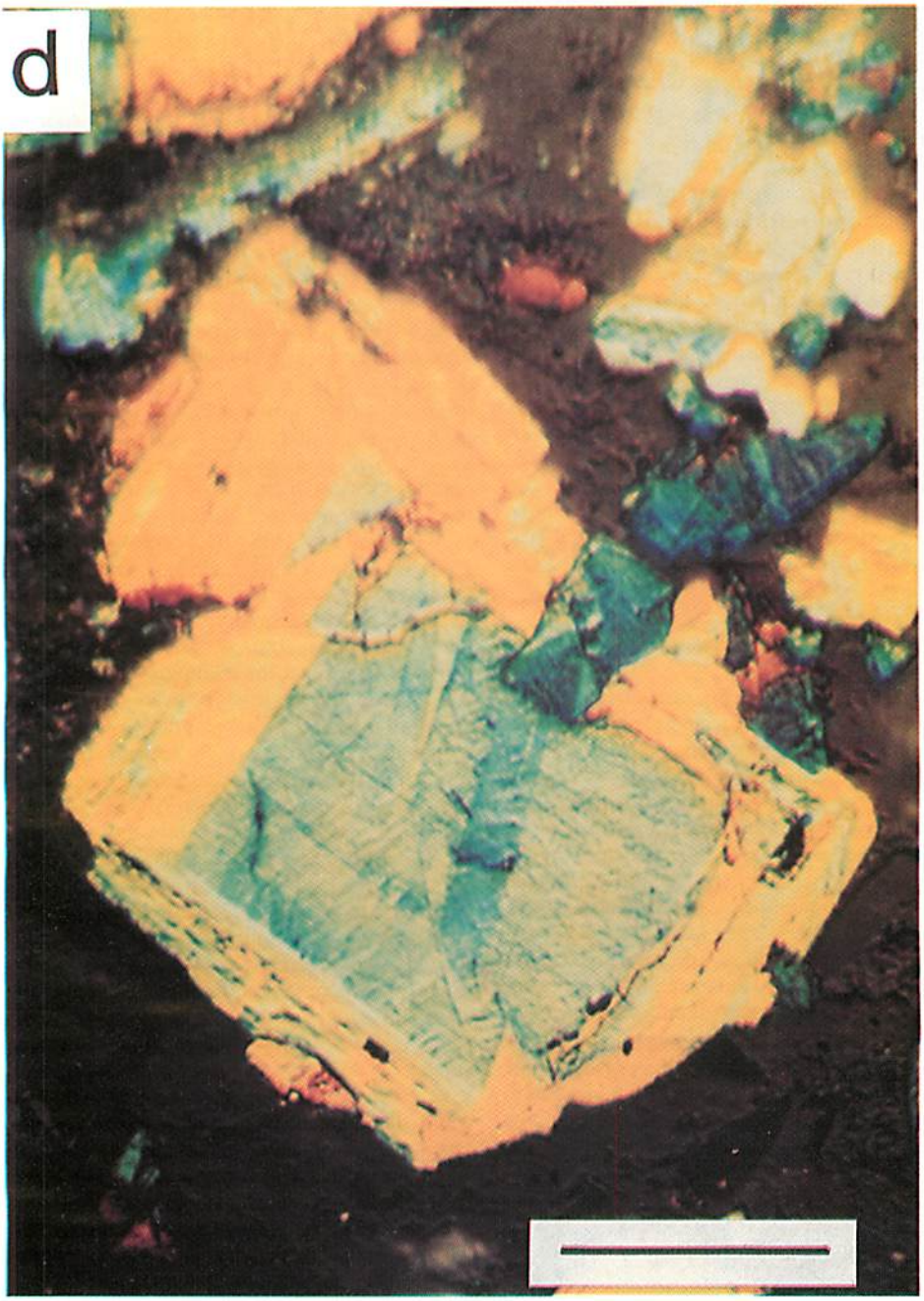

FIG. 3d. Optical micrograph of stained arsenopyrite grain from Fairview mine showing color contrast. Scale bar is 0.1 mm.

analyzed surface. The thickness of the surface layer sampled is less than about 50 Å.

XPS measurements were made using a modified Surface Science Laboratories SSX–100 X-ray photoelectron spectrometer, with a monochromatized Al$K\alpha$ X-ray source and a base pressure of 5×10^{-9} torr in the analytical chamber. The work function of the spectrometer was adjusted to give a value of 83.90 ± 0.05 eV for the Au $4f_{7/2}$ peak of metallic gold. The energy dispersion was set to give an energy difference of 857.5 ± 0.1 eV between the Cu $2p_{3/2}$ and Cu $3p$ lines. High-resolution narrow scans of the S $2p$ and C $1s$ regions were collected at 50 eV pass energy and a spot size of 300 µm. Broad scans (0–1000 eV) were accumulated with a spot size of 600 µm and a pass energy of 150 eV, conditions that give poorer resolution of energy but increased intensity. The positions of the sulfur lines were corrected for the effects of surface charging by calibration against the C $1s$ line (at 284.9 eV). The high-resolution scans were curve-fit using the software supplied by SSL. The S $2p$ line is split by spin-orbit coupling into a doublet, with components $2p_{3/2}$ and $2p_{1/2}$, separated by 1.2 eV and having a theoretical peak-area ratio in the energy spectrum of 1:1.95 (Scofield 1976). The S $2p$ spectra were curve-fit using 80% Gaussian, 20% Lorentzian peak shapes and the above energy separation and peak area constraints. A Shirley background subtraction was used. The results are summarized in Table 1 and Figure 4.

Laser Ionization Mass Spectrometry (LIMS)

A LIMA 2A laser-ionization time-of-flight mass spectrometer manufactured by Cambridge Mass Spectrometry and equipped with multiphoton postionization capabilities (MPI) was used to analyze the surface layer of stained pyrite grains exhibiting color contrast. The analytical procedure involves focussing the primary Nd–YAG laser (266 nm) on a preselected area with the help of the optical microscope attached to the sample chamber, postionization of the desorbed neutral atomic species with a second Nd–YAG laser, and analysis of the ions by time-of-flight mass spectrometry. Chryssoulis *et al.* (1992) discussed the mineralogical applications of the LIMS technique. With a focussed primary beam, the spot size is 2–5 µm in diameter. Pyrite grains from samples 17359 and 17361 from the Fairview mine were analyzed. A mass spectrum from one location in sample 17361 is shown in Figure 5, and is typical of the total of about 12 spectra acquired.

Results and Discussion

Distribution of "invisible" gold

"Invisible" gold (as defined above) was found to be generally below detection by electron microprobe (EMP) in arsenian pyrite from the Agnico-Eagle and Fairview gold deposits. However, a single fragment of an arsenian pyrite grain from Fairview mine sample 17359, which shows prominent oscillatory zoning in As content, with a broad outer margin of As-poor pyrite, yielded consistently high Au contents, up to 1400 ppm (Figs. 1c, 3b). Regions with significant Au values (>200 ppm) clearly correspond to As-rich growth zones.

These observations were elegantly confirmed by ion-probe microanalysis and ion mapping by SIMS (Figs. 1, 2b, 3c; see also Cook & Chryssoulis 1990, Chryssoulis & Cabri 1990). For the Agnico-Eagle sample (19567), ion-probe microanalysis gave Au contents of 1 to 27 ppm on two grains. High values clearly correlate with As-rich growth zones (Figs. 1a, 2b). For the Fairview sample (17359), ion-probe microanalysis gave Au values of 0.3 to 1000 ppm on four grains. Again, high values correlate with As-rich zones (Figs. 1b, 3b, c). There is not a one-to-one correspondence between the distribution of As, as presented in the micrograph of the stained grain (Fig. 3b), and the distribution of Au in the ion map (Fig. 3c). This is partly because the latter image is a composite one, and the background discrimination varied slightly from one individual ion map to another. Also, as noted below, As-rich growth bands do not always show high Au values. The grain from the Fairview mine analyzed by EMP has Au contents of 0.5 to 1000 ppm by SIMS. These results are included in Figure 1b; from the good correspondence between this figure and Figure 1c, they independently confirm the reliability of the calibrations of both Au and As in the ion-probe microanalysis by SIMS. Cabri *et al.* (1989) similarly confirmed the calibration of Au and As for Au-rich arsenopyrite from the nearby Sheba mine.

We did detect a few colloidal-size particles of Au within the As-rich zones by ion mapping by SIMS (Fig. 3c). However, the dispersed nature and even distribution of high Au values by SIMS in As-rich zones point to incorporation of much of the "invisible" gold by solid solution within the pyrite structure. Dispersed minute particles of colloidal-size Au (with particle diameters of, perhaps, 250 Å) remains a possible alternative explanation (Chryssoulis *et al.* 1987). Regardless of its precise physical form within arsenian pyrite, incorporation of the "invisible" Au must be closely associated with incorporation of the anomalous contents of As. Following Fleet *et al.* (1989), the high contents of As in arsenian pyrite appear to be present as a metastable solid-solution of the type $Fe(S,As)_2$. Gold could then be incorporated by attachment of either monoatomic ions or ionized clusters of gold atoms at sites of As-rich growth. Johan *et al.* (1989) suggested that in arsenopyrite from the Massif Central, Au substitutes for As^{3+} occupying Fe sites, but metastable incorporation on As-rich growth surfaces is a more probable mechanism of incorporation of Au in arsenian pyrite.

Griffin *et al.* (1991) suggested that the interelement

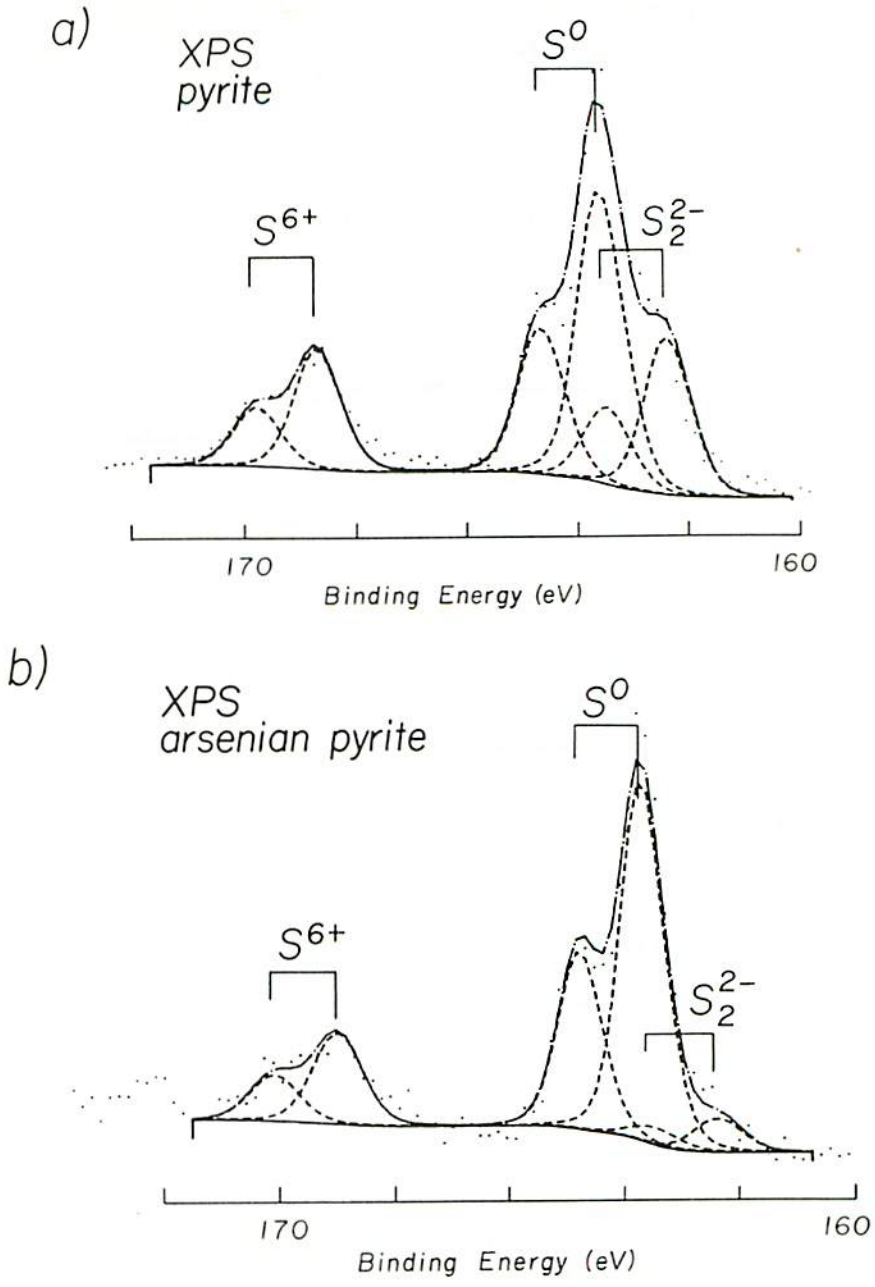

correlations they observed in As-rich pyrite from the North Arm epithermal Ag–Au deposit are consistent with a physical mixture of pyrite, arsenopyrite and a sulfosalt phase rather than atomic substitution. However, the interelement correlations of Griffin *et al.* (1991) also are consistent with substitution mechanisms, and no other evidence for the existence of inclusions of arsenopyrite and sulfosalts was presented in their study. Griffin *et al.* (1991) have misinterpreted the transmission electron microscopy (TEM) observations of Fleet *et al.* (1989). The {100} planar faults reported in the latter study are not evidence of lamellae of exsolved arsenopyrite, nor can they be interpreted as growth layers of arsenopyrite. Recent TEM study (unpublished

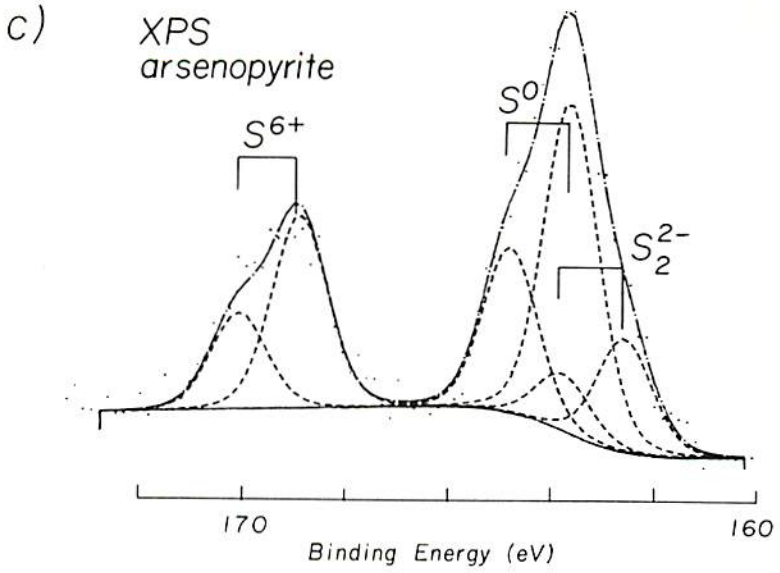

FIG. 4. X-ray photoelectron spectroscopy (XPS) spectra of S 2*p* region of polished surfaces stained with $KMnO_4$; a) As-poor pyrite (Horne mine, sample 2040); b) arsenian pyrite (Fairview mine, sample 17359); and, c) arsenopyrite (Zacatecas, sample 2486).

data) shows that {100} planar faults also are commonly present in certain samples of As-poor pyrite. Hence their presence in arsenian pyrite is probably not related to As content.

Both the SIMS and EMP data for the Fairview mine (Fig. 1) reveal that whereas high Au contents always correspond to high As, the converse correlation is not universally observed. As-rich bands do not always show high Au values. Hence, recognizing that the oscillatory-zoned microstructures of arsenian pyrite provide a record of ore-fluid evolution, it is apparent that the As-rich ore solutions were not invariably gold-bearing.

TABLE 1. SULFUR $2p_{1/2}$ BINDING ENERGIES (eV) AND FITTED PEAK WIDTHS (eV), AND TOTAL SULFUR 2p PEAK AREAS

		Binding Energy S $2p_{1/2}$	Peak Width[1]	Peak Area S 2p
PYRITE				
Horne mine, #2040:	unstained	162.8	1.24	100.0
"	stained	162.4	1.00	27.6
	(clear, metallic)	163.6	1.00	51.3
		168.7	1.00	21.0
"	stained	162.6	1.00	19.6
	(bronze, brown)	163.7	1.00	59.9
		168.2	1.00	2.5
		169.0	1.00	18.0
Unlocated, #394:	stained	162.7	0.94	21.3
	(bronze)	163.7	0.94	58.5
		169.0	0.94	20.1
ARSENIAN PYRITE				
Fairview mine, #17359:	stained	162.4	1.00	7.5
	(very light)	163.7	0.90	72.0
		169.0	1.00	20.6
ARSENOPYRITE				
Deloro, #3388:	stained	162.5	1.25	25.9
	(orange-purple)	163.6	1.25	49.5
		168.7	1.35	24.6
Zacatecos, #2486:	stained	162.6	1.25	17.7
	(red-blue)	163.6	1.25	51.7
		168.9	1.28	30.6

1 Full width at half maximum

Color staining of pyrite-group minerals with potassium permanganate

The effects of standard microchemical tests on polished surfaces of ore minerals are considered at length by Schneiderhöhn (1952) and reviewed in Cameron (1961). The present treatment of As-poor pyrite with potassium permanganate leaves the polished surface either seemingly unaffected or with a clear metallic, bronze or light brown film, the precise result apparently being dependent on orientation of the grain section. Color may appear along grain edges and fractures, especially if grain relief is present. Arsenopyrite is very reactive to the stain solution, exhibiting microstructures with strong yellow, red and blue colors (Fig. 3d) that reveal both crystallographic features (twin lamellae, grain orientation) and compositional zonation. Löllingite is either seemingly unreactive to the stain solution or rapidly tarnishes, perhaps depending on grain orientation, but does not develop colored microstructures. The S content of the present löllingite sample was not determined, and we have not investigated the effect of S-for-As substitution on the response of löllingite to the stain solution.

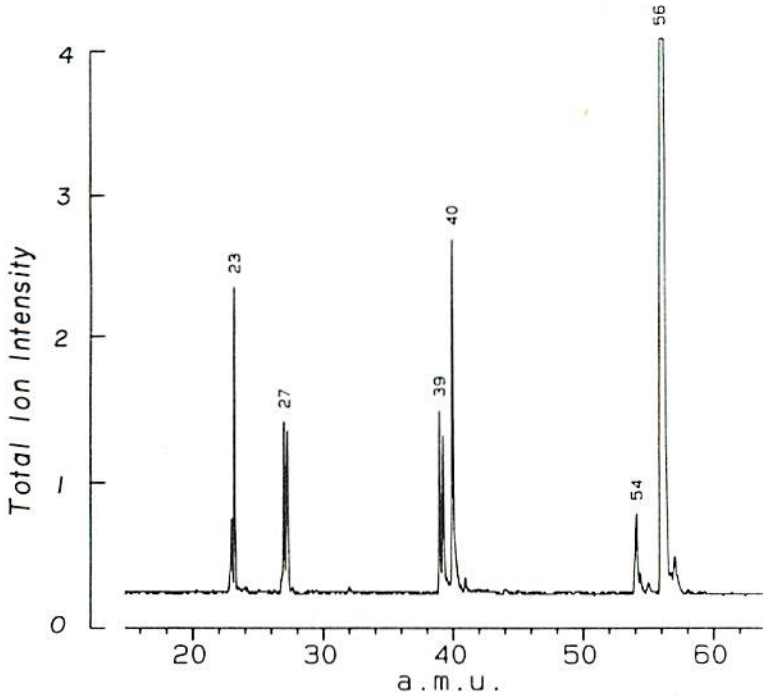

FIG. 5. Laser ionization mass spectrometry (LIMS) spectrum obtained from an As-rich band in arsenian pyrite from the Fairview mine (sample 17361) stained with $KMnO_4$; a.m.u. is atomic mass unit, and serves to identify resolved elements. Total ion intensity is in volts, and the scale is linear.

Chemistry of stained surfaces

The surface chemistry of pyrite-group minerals has been extensively investigated by XPS because of its importance to the benificiation of sulfide ores and remediation of mine wastes (*e.g.*, Brion 1980, Buckley 1987, Buckley & Woods 1987, Hyland & Bancroft 1989, Richardson & Vaughan 1989, Mycroft *et al.* 1990). In particular, the presence of elemental S can render the surface of pyrite grains strongly hydrophobic during froth flotation (see references in Buckley & Woods 1987). Fe, Mn (weak), O, N (weak), C and S were present in the broad (0–1000 eV) XPS scans of all of the pyrite-group minerals investigated in this study (namely, unstained As-poor pyrite, stained As-poor pyrite, arsenian pyrite, arsenopyrite, and löllingite). In addition, As peaks are present in the spectra of arsenopyrite and löllingite.

Overall, the high-resolution scans in the region of the S 2*p* resonances revealed S $2p_{3/2}$ peaks at about 162.6, 163.7, and 169.0 eV (Table 1), calibrated against C 1s; these binding energies are presently assigned to sulfur as disulfide (S_2^{2-}), elemental S (S^0), and sulfate (S^{6+}), respectively (Wagner *et al.* 1979, Hyland & Bancroft 1989, Mycroft *et al.* 1990). Löllingite (nominally $FeAs_2$) gave a poor S 2*p* spectrum, as expected, with only the sulfate doublet resolved above background, and spectral parameters for it are not reproduced here.

The assignment of the XPS binding energies at 163.6–163.7 eV (Table 1) to elemental S rather than polysulfide (or metal-deficient sulfide, *cf.* Buckley & Woods 1987) is based on the reference spectra cited above. It is supported by previous studies of the oxidation of pyrite surfaces that report reaction to elemental S rather than polysulfide in the presence of a strong oxidizing agent or strong acid (Buckley & Woods 1987, and references cited therein). Buckley & Woods (1987) suggested that sample temperatures below 200 K are required to prevent loss of elemental S in the ultra-high vacuum of XPS. They proposed a procedure for discrimination between elemental S and polysulfide based on corresponding measurements at both low and room temperatures. However, our SSX–100 spectrometer was not equipped for low-temperature measurements. In the absence of low-temperature measurements, and recognizing that the binding energies in question are on the low side of the range of values associated with elemental S (163.6–164.1 eV), there

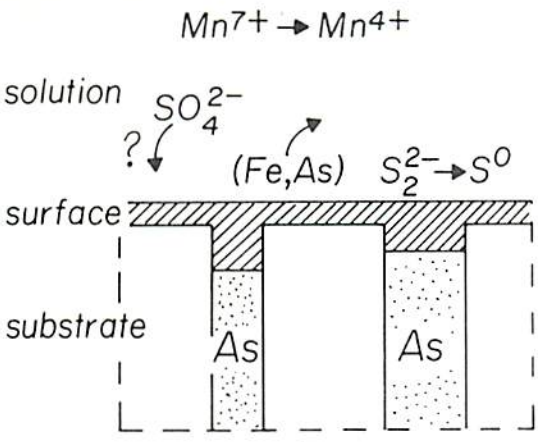

FIG. 6. Schematic cross-section through surface of grain of arsenian pyrite reacted with potassium permanganate solution (see text); hatched area is dominantly elemental S; As indicates As-rich growth band.

remains the possibility that the dominant S species in the stained surfaces is, rigorously, a very metal-deficient polysulfide rather than elemental S.

The disulfide S 2*p* doublet in the XPS spectra clearly reflects disulfide groups from the unoxidized substrate of the pyrite specimens (Table 1, Figs. 4, 6, Hyland & Bancroft 1989, Mycroft *et al.* 1990). This appears to be confirmed by the absence of reduced species of sulfur in the spectrum of löllingite. However, on this basis, the disulfide S 2*p* doublet in the spectra of the arsenopyrite (Table 1, Fig. 4) is unexplained, but could represent reorganization of ligand atoms in near-surface layers following preferential leaching of As (see Buckley 1987).

The sulfate present in the spectra may have been adsorbed from the stain solution, with evidence again from the spectrum of löllingite. However, it could also be a final product of the step-wise oxidation of the substrate (see Brion 1980, and below).

The dominant elemental S component of the surface layers is clearly a product of the oxidation of disulfide (S_2^{2-}) and sulfarsenide [$(AsS)^{3-}$] in the substrate. On pyrite surfaces, the yield of elemental S increases with As-for-S substitution, as is well illustrated by the progression of spectra from unstained As-poor pyrite to stained As-poor pyrite and stained arsenian pyrite (Table 1, Fig. 4). Arsenic-for-S substitution appears to promote the surface oxidation of pyrite by potassium permanganate solution. We were not able to investigate the correlation of elemental S with As content within individual arsenian pyrite microstructures because of the limited spatial resolution of XPS (300 μm in this study).

Sporadic development of color along the edges of As-poor pyrite grains is readily attributable to the greater proportion of broken bonds there, which would tend to promote oxidation of the substrate (*cf.* McKibben & Barnes 1986). For arsenian pyrite and arsenopyrite, there is some progression of color development with reaction time, but with protracted exposure, all surfaces become corroded.

As discussed above, we did not observe compelling evidence for polysulfide species in the XPS spectra. Polysulfides were reported by Mycroft *et al.* (1990) as a result of the electrochemical oxidation of pyrite surfaces in near-neutral aqueous chloride electrolytes at 600 to 700 mV (*i.e.*, at redox conditions equivalent to those of some aerated surface waters). Redox potentials were not monitored in the present study, but for oxidation with permanganate, they would have been somewhat higher than in the electrochemical study of Mycroft *et al.* (1990). Higher redox potentials might explain the absence of intermediate products of oxidation in the present study. Hamilton & Woods (1981) studied the electrochemistry of pyrite as a function of pH in aqueous solution. They reported that yields of elemental S are higher at lower pH, and that elemental S oxidizes to sulfate above 800 mV. Thus, partial oxidation to sulfate could have occurred in the present staining experiments, leaving the origin of the surface sulfate component questionable.

In general, the oxidation products of pyrite surfaces are only approximately consistent with equilibrium stability of the solid phases and dissolved species at room temperature (see Mycroft *et al.* 1990), which are familiarly depicted in Pourbaix (Eh–pH) diagrams (*e.g.*, Garrels & Christ 1965). This is because oxidation of sulfide species to sulfate is complex, with numerous potential intermediary oxidation states, some of which involve rate-controlling steps. Also, for surface oxidation, the reaction rate is expected to decrease when film thickness reaches a few thousand ångströms as the transport of reactive species through the film becomes rate-controlling. Buckley & Woods (1987) noted that a thin surface-layer of sulfur (considered to be polysulfide) effectively passivated pyrite from attack by acetic acid. Whereas elemental S is an important product of oxidation with permanganate, and polysulfide appears by electrochemical oxidation (Mycroft *et al.* 1990), elemental S is not an important product of oxidation of pyrite when it is exposed to air (Brion 1980, Buckley & Woods 1987). It appears that a strong oxidizing agent or strong acid may be required for the formation of elemental S (*cf.* Buckley & Woods 1987), causing oxidation to be initially rapid but later inhibited by the build-up of film thickness. In the present microchemical procedure, it is unlikely that the drop of permanganate solution equilibrated with the partially oxidized surface of pyrite. The permanganate appears to have been reduced to MnO_2; the half-cell potentials for Mn^{4+} species are substantially above those for S^0 species (see Garrels & Christ 1965).

The present application of LIMS was preliminary.

Only Na, Al, K, Ca, Fe and Mn (trace) are present in the LIMS spectra of positive atomic species of stained arsenian pyrite from the Fairview mine (Fig. 5). However, this study serves to illustrate the extraordinary sensitivity of this technique, because Na, Al, K, and Ca were almost certainly sorbed from the wash solution (tap water). The dominant Fe signature in the LIMS spectra reflects surface Fe atoms from the surface oxidation of the pyrite substrate.

Origin of the stain color

Our study of the chemistry of polished surfaces stained with potassium permanganate solution was directed to an understanding of the nature of the characteristic color of the stain. This is possibly attributable to a chromophore substance (*e.g.*, a Mn species), but this explanation seems to be precluded by the wide range of colors observed. Alternatively, the colors could be attributable to a surface film causing optical interference. This explanation seems to be favored because the characteristic colors are analogous to the first-order colors of optical interference. The active film might then be either MnO_2 precipitated from the stain solution or a product of the surface oxidation of the substrate.

The XPS and LIMS studies clearly show that Mn is present in only trace quantities in the surface layers of the pyrite-group minerals investigated, and therefore a Mn compound could not be responsible for the characteristic colors. However, elemental S is present in quantity at the surface, and moreover, the amount present on pyrite surfaces is proportional to As-for-S substitution. This correlation is quite significant, because it links color development with the distribution of As and "invisible" Au. The surface oxidation of oscillatory-zoned arsenian pyrite by potassium permanganate solution is depicted schematically in Figure 6, which shows the preferential leaching of Fe and As, oxidation of disulfide to elemental S, which remains as a film with thickness proportional to the As content of the immediate substrate, and the irregular etched interface between the substrate and surface film.

From the theory for interference by thin films in reflection (*e.g.*, Heavens 1965), interference colors for white light in normal incidence are given by:

$$m\lambda = 2nd\cos\phi, \qquad (2)$$

where m is order, λ is wavelength (color), d is film thickness, n is index of refraction of the film, and ϕ is angle of incidence; this expression ignores the effects of differential absorption and assumes that the indices of refraction increase in the sequence air < film < pyrite (*i.e.*, $n_{air} < n < n_{pyrite}$). Hence, color development is related to thickness of surface film, and first-order colors require a film thickness of elemental S of only about 0.2 μm. This thickness is similar to the depth of etching estimated optically from cleaned stained surfaces. The color of the stain is observed to fade when the surface is wetted with water. This phenomenon is reversible and must be related to additional interference associated with the air–water interface. The progressive (nonreversible) fading of the stain color when exposed to air over a period of several days is readily attributable to aging of the surface film of elemental S, possibly by hydrolysis or oxidation to sulfate (see Brion 1980, Buckley 1987). Final confirmation of the interference-related nature of the stain color was obtained by a simple experiment with arsenopyrite. When a stained polished surface was allowed to fade through aging and then lightly wiped with a new scalpel blade, the surface became streaked with lower-order colors. Clearly, the scalpel blade scoured and scratched the surface film, removing (or reorganizing) the outer aged layer and causing variation in thickness.

Finally, XPS does not probe beyond the outer 30 to 50 Å of the sample surface, yet the present explanation for stain color requires a film thickness of elemental S of about 2000 Å. The disulfide component in the XPS spectra then must represent isolated particles of unoxidized substrate within the surface layer or a very irregular interface between the substrate and surface layer, much more irregular than that depicted in Figure 6.

Acknowledgements

We thank Y. Moëlo and D.J. Vaughan for constructive reviews, R.F. Martin and E. Makovicky for editorial assistance, I.J. Muir for helpful discussion, R.L. Barnett for assistance with electron-microprobe analysis, J. Forth for polished sections, NSERC for financial support (operating grant to MEF), and Surface Science Western for instrument time.

References

Arnold, M. (1981): Cristallogenèse et géochimie isotopique de la pyrite: apports à la métallogenèse des amas sulfurés associés à un volcanisme sous-marin. *Annales de l'École Nationale Supérieure de Géologie Appliquée et de Propection Minière de Centre de Recherches Pétrographiques et Géochimiques (C.N.R.S.) et des Laboratoires des Sciences de la Terre de l'Université Nancy (France), Sciences de la Terre, Mém.* **40**.

Barnett, E.S., Hutchinson, R.W., Adamcik, A. & Barnett, R.L. (1982): Geology of the Agnico-Eagle gold deposit, Quebec. *In* Precambrian Sulphide Deposits (R.W. Hutchinson, C.D. Spence & J.M. Franklin, eds.). *Geol. Assoc. Can., Spec. Pap.* **25**, 403-426.

Barton, P.B., Jr. & Bethke, P.M. (1987): Chalcopyrite disease in sphalerite: pathology and epidemiology. *Am. Mineral.* **72**, 451-467.

_____, _____ & Roedder, E. (1977): Environment of ore

deposition in the Creede mining district, San Juan Mountains, Colorado. III. Progress toward interpretation of the chemistry of the ore-forming fluid for the OH vein. *Econ. Geol.* **72**, 1-24.

BRIGGS, D. & SEAH, M.P. (1983): *Practical Surface Analysis.* John Wiley and Sons, New York.

BRION, D. (1980): Étude par spectroscopie de photoélectrons de la dégradation superficielle de FeS_2, $CuFeS_2$, ZnS et PbS à l'air et dans l'eau. *Appl. Surface Sci.* **5**, 133-152.

BUCKLEY, A.N. (1987): The surface oxidation of cobaltite. *Aust. J. Chem.* **40**, 231-239.

_____ & WOODS, R. (1987): The surface oxidation of pyrite. *Appl. Surface Sci.* **27**, 437-452.

BURKART-BAUMANN, I. & OTTEMANN, J. (1971): Arsenführende Pyrite mit Bravoit-ähnlichen Strukturen. *Mineral. Deposita* **6**, 148-152.

CABRI, L.J., CHRYSSOULIS, S.L., CAMPBELL, J.L. & TEASDALE, W.J. (1991): Comparison of in-situ gold analyses in arsenian pyrite. *Appl. Geochem.* **6**, 225-230.

_____, _____, DE VILLIERS, J.P.R., LAFLAMME, J.H.G. & BUSECK, P.R. (1989): The nature of "invisible" gold in arsenopyrite. *Can. Mineral.* **27**, 353-362.

CAMERON, E.N. (1961): *Ore Microscopy.* John Wiley & Sons, New York.

CHRYSSOULIS, S.L. (1990): Quantitative trace precious metal analysis of sulphide and sulpharsenide minerals by SIMS. *In* Secondary Ion Mass Spectrometry SIMS VII (A. Benninghoven, C.A. Evans, K.D. McKeegan, H.A. Storms & H.W. Werner, eds.). John Wiley and Sons, New York (405-408).

_____ & CABRI, L.J. (1990): Significance of gold mineralogical balances in mineral processing. *Trans. Inst. Min. Metall. (Sect. C: Mineral Process. Extr. Metall.)* **99**, C1-C10.

_____, _____ & SALTER, R.S. (1987): Direct determination of "invisible" gold in refractory sulphide ores. *In* Proc. Int. Symp. on Gold Metallurgy – Refractory Gold **1** (R.S. Salter, D.M. Wyslouzil & G.W. McDonald, eds.). Pergamon Press, New York, (235-244).

_____, STOWE, K.G.& REICH, F. (1992): Characterization of composition of mineral surfaces by laser-probe microanalysis. *Trans. Inst. Min. Metall. (Sect. C: Mineral Process. Extr. Metall.)* **100**, C1-C6.

_____ & WEISENER, C.G. (1991): Quantification and imaging of submicroscopic Au in ore minerals by SIMS. *In* Secondary Ion Mass Spectrometry SIMS VIII (A. Benninghoven, K.T.F. Janssen, J. Tümpner & H.W. Werner, eds.). John Wiley and Sons, Chichester, U.K. (517-520).

COOK, N.J. & CHRYSSOULIS, S.L. (1990): Concentrations of "invisible gold" in the common sulfides. *Can. Mineral.* **28**, 1-16.

FLEET, M.E., MACLEAN, P.J. & BARBIER, J. (1989): Oscillatory-zoned As-bearing pyrite from strata-bound and stratiform gold deposits: an indicator of ore fluid evolution. *In* The Geology of Gold Deposits: The Perspective in 1988 (R.R. Keays, W.R.H. Ramsay & D.I. Groves, eds.). *Econ. Geol., Monogr.* **6**, 356-362.

GARRELS, R.M. & CHRIST, C.L. (1965): *Solutions, Minerals, and Equilibria.* Harper & Row, New York.

GRIFFIN, W.L., ASHLEY, P.M., RYAN, C.G., SIE, S.H. & SUTER, G.F. (1991): Pyrite geochemistry in the North Arm epithermal Ag–Au deposit, Queensland, Australia: a proton-microprobe study. *Can. Mineral.* **29**, 185-198.

HAMILTON, I.C. & WOODS, R. (1981): An investigation of surface oxidation of pyrite and pyrrhotite by linear potential sweep voltammetry. *J. Electroanal. Chem.* **118**, 327-343.

HEAVENS, O.S. (1965): *Optical Properties of Thin Solid Films.* Dover, New York.

HYLAND, M.M. & BANCROFT, G.M. (1989): An XPS study of gold deposition at low temperature on sulphide minerals: reducing agents. *Geochim. Cosmochim. Acta* **53**, 367-372.

JEAN, G.E. & BANCROFT, G.M. (1985): An XPS and SEM study of gold deposition at low temperatures on sulphide mineral surfaces: concentration of gold by adsorption/reduction. *Geochim. Cosmochim. Acta* **49**, 979-987.

JOHAN, Z., MARCOUX, E. & BONNEMAISON, M. (1989): Arsénopyrite aurifère: mode de substitution de Au dans la structure de FeAsS. *C.R. Acad. Sci. Paris* **308**, *Sér.* II, 185-191.

MACLEAN, P.J. (1991): *Characterization of Pyrite from Gold Deposits.* Ph.D. thesis, University of Western Ontario, London, Ontario.

_____ & FLEET, M.E. (1989): Detrital pyrite in the Witwatersrand gold fields of South Africa: evidence from truncated growth banding. *Econ. Geol.* **84**, 2008-2011.

MCINTYRE, N.S. (1984): Modern methods of surface analysis and microanalysis. *In* Environmental Geochemistry (M.E. Fleet, ed.). *Mineral. Assoc. Can., Short-Course Handbook* **10**, 169-195.

MCKIBBEN, M.A. & BARNES, H.L. (1986): Oxidation of pyrite in low temperature acidic solutions: rate laws and surface textures. *Geochim. Cosmochim. Acta* **50**, 1509-1520.

MYCROFT, J.R., BANCROFT, G.M., MCINTYRE, N.S., LORIMER, J.W. & HILL, I.R. (1990): Detection of sulphur and polysulphides on electrochemically oxidized pyrite surfaces by X-ray photoelectron spectroscopy and Raman spectroscopy. *J. Electroanal. Chem.* **292**, 139-152.

RICHARDSON, S. & VAUGHAN, D.J. (1989): Arsenopyrite: a

spectroscopic investigation of altered surfaces. *Mineral. Mag.* **53**, 223-229.

SCHNEIDERHÖHN, H. (1952): *Erzmikroskopisches Praktikum*. E. Schweizerbart'sche Verlagsbuchhandlung, Stuttgart, Germany.

SCOFIELD, J.H. (1976): Hartree–Slater subshell photoionization cross-sections at 1254 and 1486 eV. *J. Electron Spectros. Related Phenom.* **8**, 129-137.

WAGNER, C.D., RIGGS, W.M., DAVIS, L.E. & MOULDER, J.F. (1979): *Handbook of X-ray Photoelectron Spectroscopy* (G.E. Muilenberg, ed.). Perkin-Elmer Corp., Eden Prairie, Minnesota.

WIGGETT, B.S.A., BRINK, W.C.J. & VORSTER, M.A. (1986): The Fairview gold mine, Barberton greenstone belt. *In* Mineral Deposits of Southern Africa **1** (C.R. Anhaeusser & S. Maske, eds.). *Geol. Soc. S. Afr.*, 169-179.

Received November 7, 1991, revised manuscript accepted March 21, 1992.